Electronic Supplementary Information for:

Tricolour Luminescence in Au(I) Complex Controlled by Polymorphism and Mechanical Stress

Andriani Furoida,[a] Misato Daitani,[a] Kohsuke Matsumoto,[a] Kyohei Hisano,[a,b] and Osamu Tsutsumi[a*]

[a] *Department of Applied Chemistry, Ritsumeikan University. 1-1-1 Nojihigashi, Kusatsu 525-8577, Japan.*
[b] *Present address: Laboratory for Chemistry and Life Science, Institute of Innovative Research, Tokyo Institute of Technology, 4259 Nagatsuta, Midori-ku, Yokohama 226-8501, Japan.*

* Correspondence should be addressed to O. Tsutsumi.
E-mail: tsutsumi@sk.ritsumei.ac.jp

Table of contents

1. NMR characterization ••••••••••••S-3
2. X-ray crystallography ••••••••••••S-5
3. Thermal properties ••••••••••••S-7
4. Photophysical properties ••••••••••••S-11
5. Powder XRD analysis ••••••••••••S-12
6. TD-DFT calculation ••••••••••••S-14
7. Mechanochromic luminescence ••••••••••••S-15
8. Luminescence in LC phase ••••••••••••S-19
9. References ••••••••••••S-20

1. NMR characterization

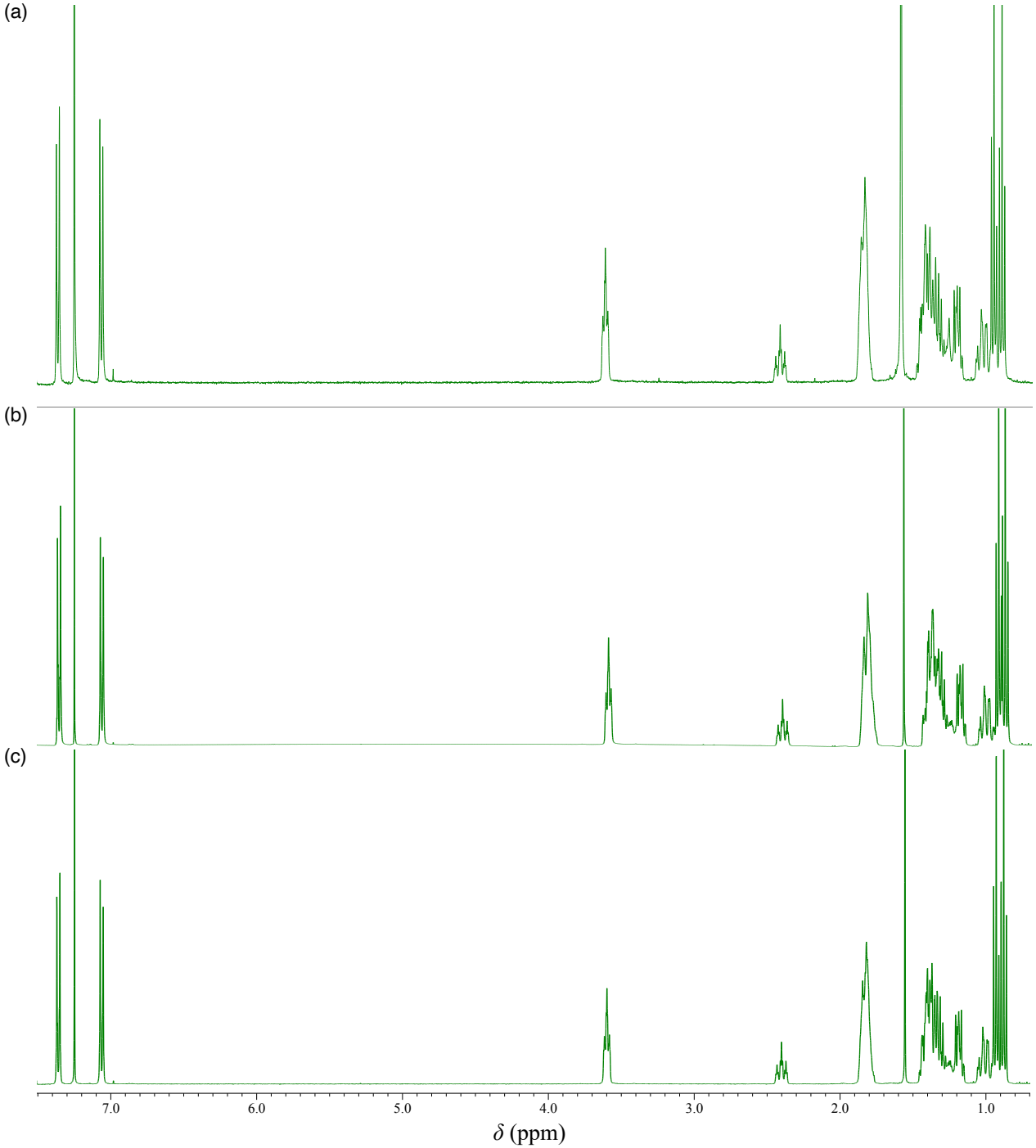

Fig. S1 ^{1}H NMR spectra of **CP** polymorphs in $CDCl_3$ solution: (a) **CP-B**, (b) **CP-G**, (c) **CP-Y**.

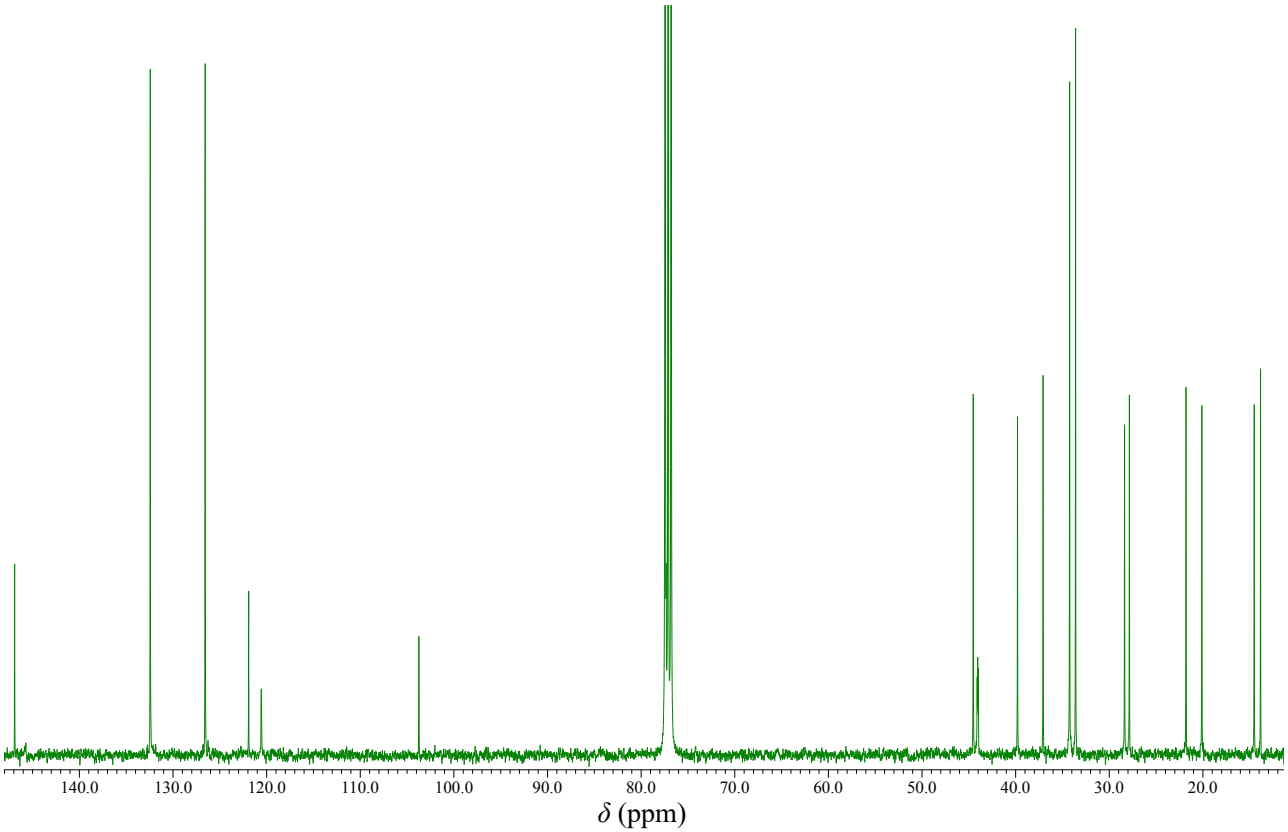

Fig. S2 ^{13}C NMR spectrum of **CP** in $CDCl_3$.

2. X-Ray Crystallography

Single crystals were obtained by slow evaporation from a mixed solvent system of dichloromethane as good solvent and hexane or ethyl acetate as poor solvent. The X-ray diffraction measurement was carried out at room temperature (293 K). The crystal packing of **CP** polymorphs is shown in Fig. S3 with the crystal data disclosed in Table S1 have been indexed, and are included in the Cambridge Crystallographic Center (CCDC) database with the following reference numbers: CCDC 2327717 (**CP-B**), CCDC 2327718 (**CP-G**), and CCDC 2327741 (**CP-Y**). The indexed database contains additional supplementary crystallographic data for this paper and may be accessed without charge at http://www.ccdc.cam.ac.uk/conts/retrieving.html.

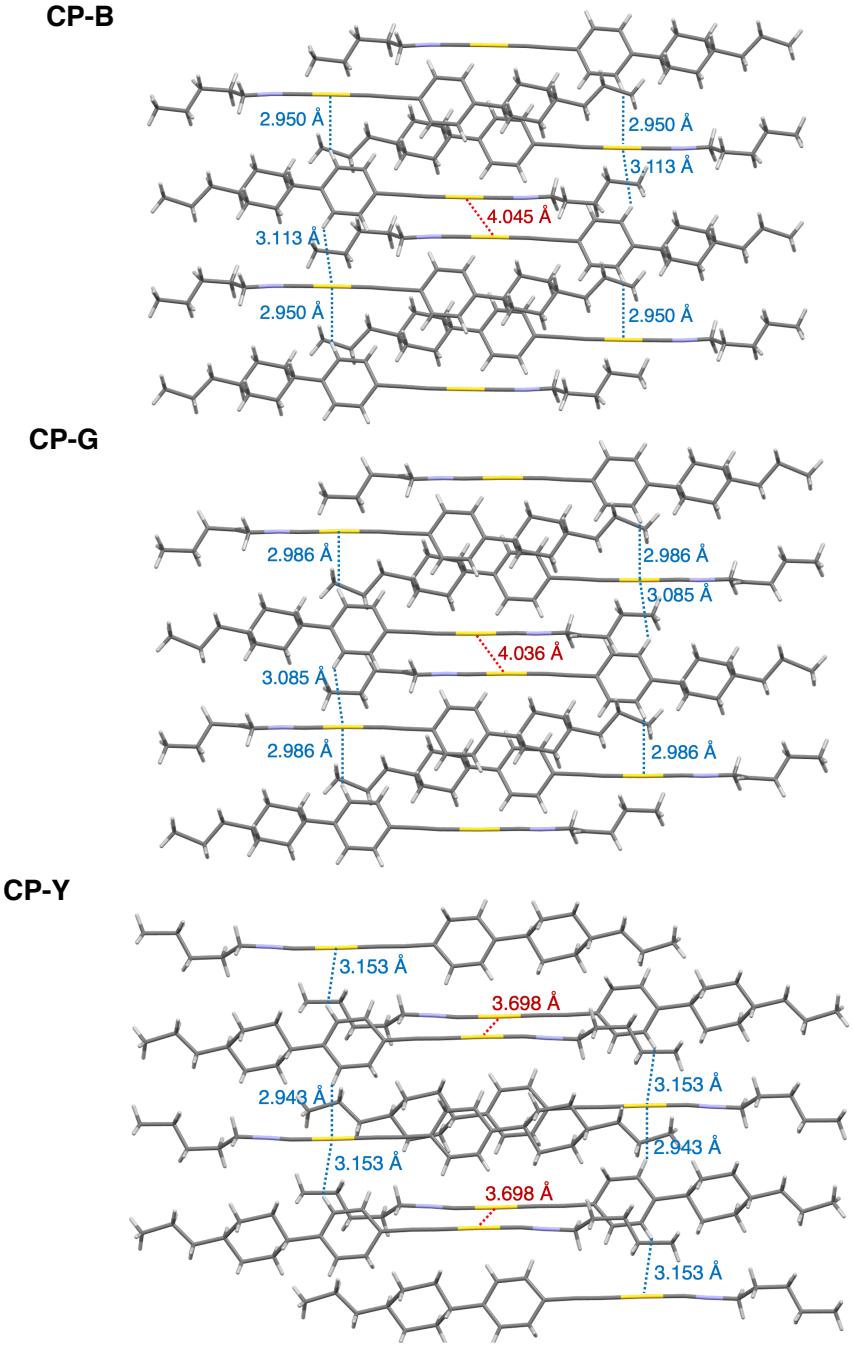

Fig. S3 Crystal packing structures of **CP** at room temperature. Color legend: grey, C; white, H; blue, N; yellow, Au. Intermolecular Au–Au and CH–Au interactions are indicated with red and blue dashed lines, respectively.

Table S1. Crystallographic data of **CP** crystal polymorphs.

	CP-B	**CP-G**	**CP-Y**
Empirical Formula	$C_{23}H_{32}AuN$	$C_{23}H_{32}AuN$	$C_{23}H_{32}AuN$
Formula Weight	519.484	519.484	519.484
Temperature (K)	293 K	293 K	293 K
Crystal Colour / Habit	colourless, plate	colourless, plate	colourless, plate
Crystal Size (mm)	0.6 × 0.5 × 0.3	0.7 × 0.5 × 0.3	0.6 × 0.5 × 0.2
Crystal System	triclinic	triclinic	triclinic
Space group	*P*–1	*P*–1	*P*–1
a (Å)	9.197 (9)	9.210 (2)	9.196 (3)
b (Å)	9.965 (10)	9.984 (3)	9.937 (4)
c (Å)	13.627 (14)	13.584 (3)	13.588 (5)
α (°)	68.895 (4)	68.792 (10)	68.902 (12)
β (°)	89.895 (4)	89.793 (9)	89.871 (11)
γ (°)	72.389 (3)	72.379 (7)	72.413 (11)
V (Å^3)	1102.4 (2)	1101.9 (5)	1096.4 (7)
Z	2	2	2
$R\ [F^2 > 2\sigma\ (F^2)]$	0.0476	0.1054	0.0742
$wR(F^2)$	0.2047	0.3512	0.2076

CheckCIF reports

CheckCIF reports indicate several level A alerts, primarily stemming from the quality of single crystals. Despite our significant efforts to enhance crystal quality, obtaining higher quality crystals for **CP-G** and **CP-Y** remains challenging because those are not the thermodynamically most stable crystal structure. As a result, the reported results represent the best achievable outcome at present. The explanations for each alert are as follows:

CheckCIF report for CP-G dataset:

1. **PLAT029_ALERT_3_A**: The crystal exhibited poor diffraction quality due to the poor crystal quality, leading to low data completeness. Despite our efforts to enhance crystal quality, this represents the best achievable result.
2. **PLAT234_ALERT_4_A**: A notable Hirshfeld difference in the C–C bond may be attributed to conformational flexibility and partial disorder of the alkyl chain, compounded by limitations in data quality. While measuring diffraction at low temperature could potentially mitigate conformational flexibility and partial disorder, it is essential to maintain consistency in measurement conditions to observe the crystal structure associated with the luminescence behaviour accurately.
3. **PLAT721_ALERT_1_A**: Deviations in bond lengths may be attributed to data quality limitations, affecting the precise localization of hydrogen atoms.

CheckCIF report for CP-Y dataset:

1. **PLAT029_ALERT_3_A**: The crystal exhibited poor diffraction quality, resulting in low data completeness. Despite our efforts to improve crystal quality, this represents the best achievable result.
2. **PLAT234_ALERT_4_A**: Notable Hirshfeld differences in the N–C and C–C bonds may be attributed to conformational flexibility and partial disorder of the alkyl chain, compounded by limitations in data quality. While measuring diffraction at low temperature could potentially mitigate conformational flexibility and partial disorder, it is essential to maintain consistency in measurement conditions to observe the crystal structure associated with the luminescence behaviour accurately.
3. **PLAT721_ALERT_1_A**: Observed deviations in bond lengths and angles may be attributed to limitations in data quality, impacting the precise localization of hydrogen atoms.

3. Thermal properties

Thermal stability of **CP** was evaluated by thermogravimetric analysis (TGA; Shimadzu, DTG-60AH) under N_2 atmosphere at a heating rate of 5.0 °C min^{-1} in the range of 25–600 °C. (Fig. S4). The phase transition behavior was observed using differential scanning calorimetry (DSC) (X-DSC7000, SII) at a scanning rate of 1 °C min^{-1} (Figs. S5–S6).

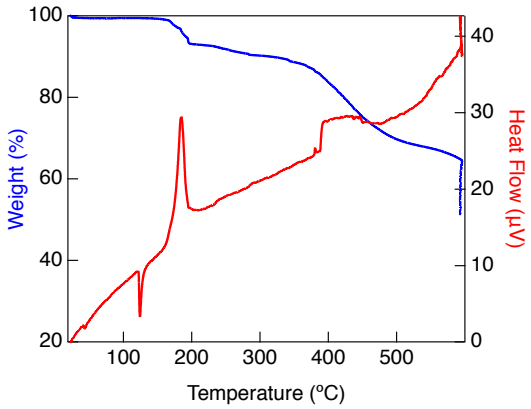

Fig. S4 TG-DTA thermograms of **CP** under N_2 atmosphere. Heating rate was 5.0 °C min^{-1}.

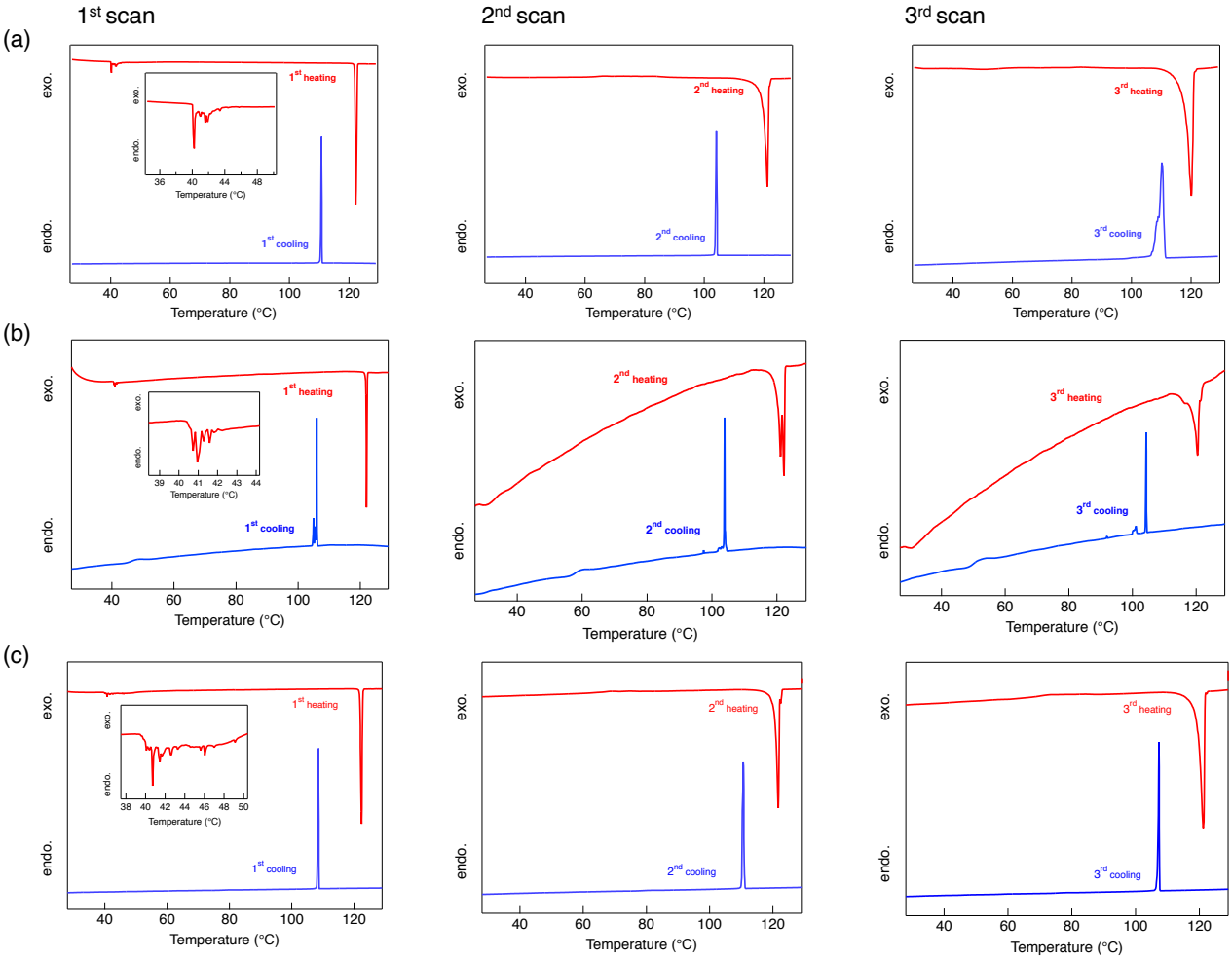

Fig. S5 DSC thermograms of (a) **CP-B**, (b) **CP-G**, and (c) **CP-Y** in the first, second, and third scan (scanning rate: 1 °C min^{-1}; red, heating; blue, cooling).

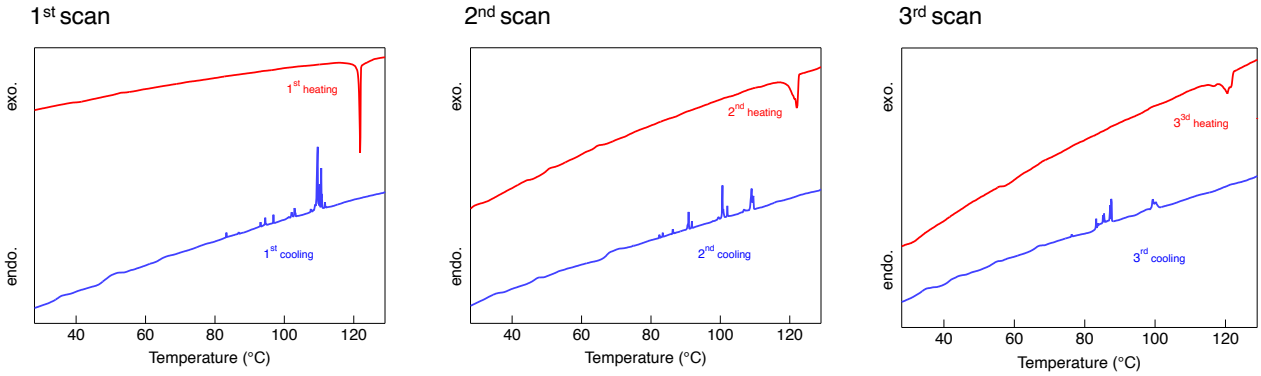

Fig. S6 DSC thermograms of $\mathbf{CP_{ground}}$ in the first, second and third scan (scanning rate: 1 °C min^{-1}; red: heating, blue: cooling).

Table S2. Thermal properties of **CP** crystal polymorphs.

		Phase sequences (°C)[a,b]	T_{dec} (°C)[c]
CP-B	Heating	Cr_1 40 Cr_2 122 N	186
	Cooling	Cr_2 110 N	
CP-G	Heating	Cr_1 40 Cr_2 122 N	
	Cooling	Cr_2 106 N	
CP-Y	Heating	Cr_1 40 Cr_2 122 N	
	Cooling	Cr_2 108 N	
$\mathbf{CP_{ground}}$	Heating	Cr_1 121 N	
	Cooling	Cr_x 110 N	

[a] Abbreviations: Cr, crystalline; N, nematic. [b] The phase transition temperature was determined by DSC as the peak onset. [c] Thermal decomposition temperature was determined by TGA at a heating rate of 5.0 °C min^{-1}.

4. Photophysical properties

Luminescence properties in degassed solution

The sample solutions (1.5×10^{-6} and 1×10^{-5} mol L^{-1}) in THF (f_w = 0%) and water/THF mixed solvent (f_w = 80%) were prepared and put into a sealed cell. The capillary was inserted into the cell and the argon gas was slowly bubbled into the solution for 15–20 minutes. After degassing, the capillary was removed, and the cell should be kept in a close system when measuring photoluminescence.

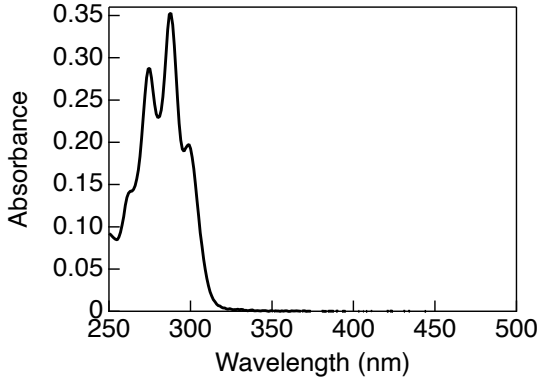

Fig. S7 Absorption spectrum of **CP** in THF ([**CP**] = 1×10^{-5} mol L^{-1}).

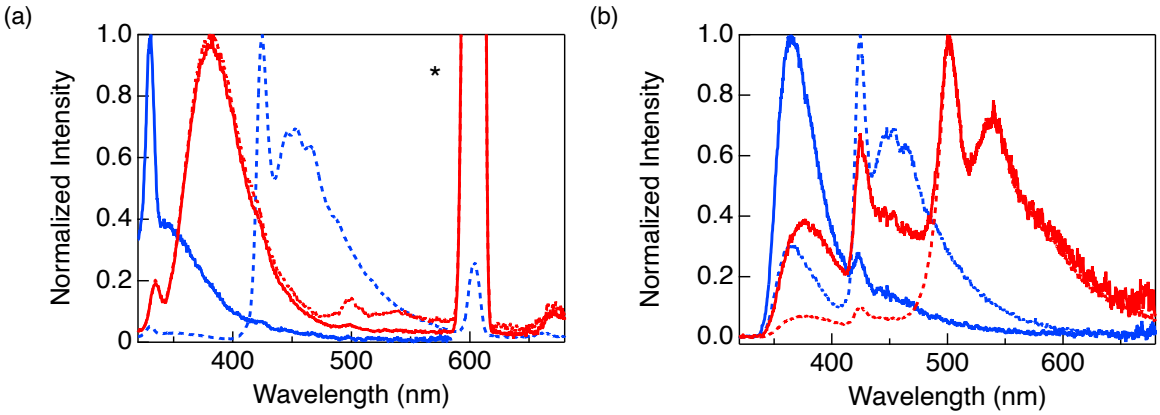

Fig. S8 Luminescence spectra of **CP** in THF/water mixtures with f_w = 0% (blue) and 80% (red) under different **CP** concentrations: (a) [**CP**] = 1.5×10^{-6} mol L^{-1}, (b) [**CP**] = 1×10^{-5} mol L^{-1}. Solid lines represent spectra before Ar bubbling, while dashed lines represent spectra after Ar bubbling. λ_{ex} = 300 nm. * denotes the second-order diffraction of the excitation light.

Photoluminescence lifetime in degassed solution

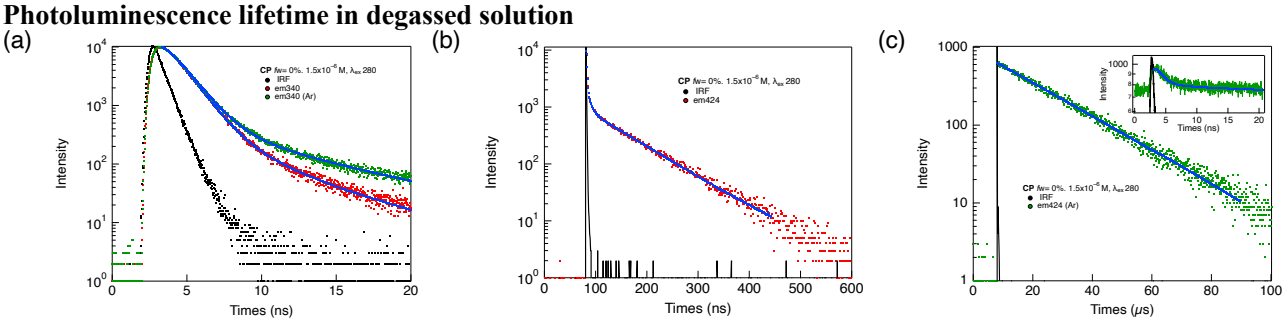

Fig. S9 Luminescence decay profiles of **CP** in THF without water before and after Ar bubbling ([**CP**] = 1.5×10^{-6} mol L^{-1}, λ_{ex} = 280 nm): red, observed decay before bubbling; green, observed decay after Ar bubbling; blue, fitting curve; black, instrument response function. (a) monitored at 340 nm (band I), (b) monitored at 424 nm (band II) under ambient air, (c) monitored at 424 nm (band II) after Ar bubbling.

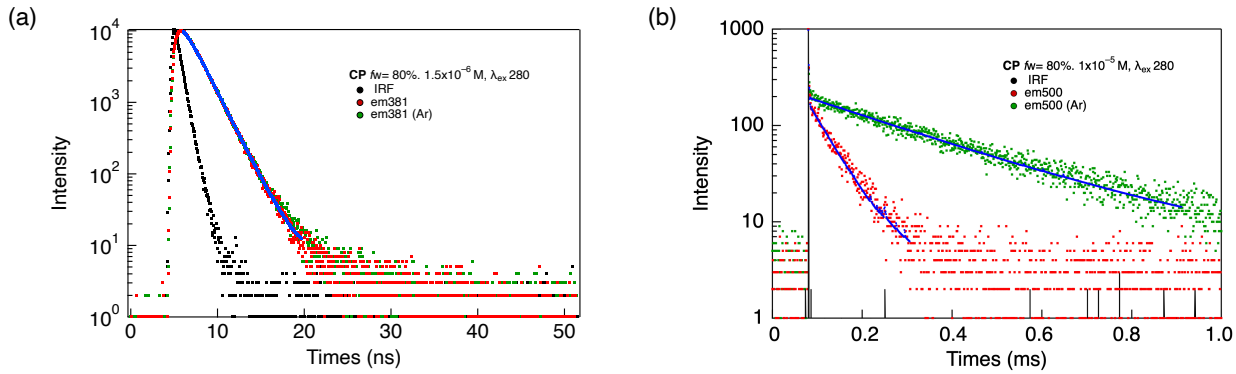

Fig. S10 Luminescence decay profiles of **CP** in THF/water mixture (f_w = 80%) before and after Ar bubbling ([**CP**] = 1.5×10^{-6} mol L^{-1} for (a) and 1×10^{-5} mol L^{-1} for (b), λ_{ex} = 280 nm): red, observed decay before bubbling; green, observed decay after Ar bubbling; blue, fitting curve; black, instrument response function. (a) monitored at 381 nm, (b) monitored at 500 nm.

Table S3. Luminescence lifetime of **CP** in THF/water mixed solvent. [a]

f_w	λ_{obs} (nm), luminescence band	τ	Ar bubbling
0%	340, band I	~1 ns (98%) 4 ns (2%)	No
		~1 ns (97%) 7 ns (3%)	Yes
	424, band II	~1 ns (90%) 6 ns (6%) 80 ns (4%)	No
		~1 ns (1%) 17 μs (99%)	Yes
80%	381, band I	~1 ns	No
		~1 ns	Yes
	500, band III	0.5 μs (94%) 49 μs (6%)	No
		0.6 μs (95%) 271 μs (5%)	Yes

[a] Abbreviations: f_w, volume fraction of water in the mixed solvent; λ_{obs}, observation wavelength for luminescence decay; τ, luminescent lifetime. λ_{ex} = 280 nm for all measurements.

Photoluminescence of crystal polymorphs at different excitation

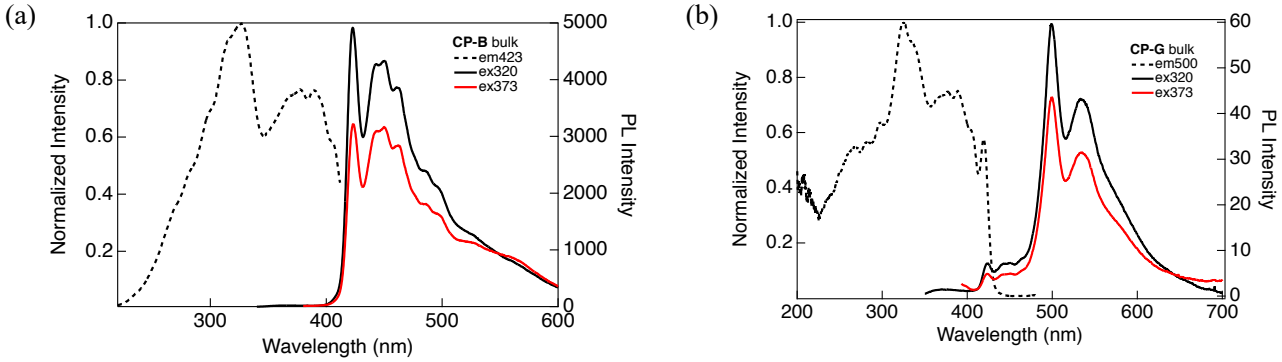

Fig. S11 Excitation (dashed line) and emission spectra (solid line) of (a) **CP-B** and (b) **CP-G** in the bulk crystals at different excitation at room temperature. (black: λ_{ex} = 320 nm; red: λ_{ex} = 373 nm).

Photoluminescence lifetime of crystal polymorphs

Photoluminescence decay profiles of **CP** crystals were measured by using Quantaurus-Tau (Hamamatsu), λ_{ex} = 340 nm, frequency; 2 kHz, stop condition; 1000 counts.

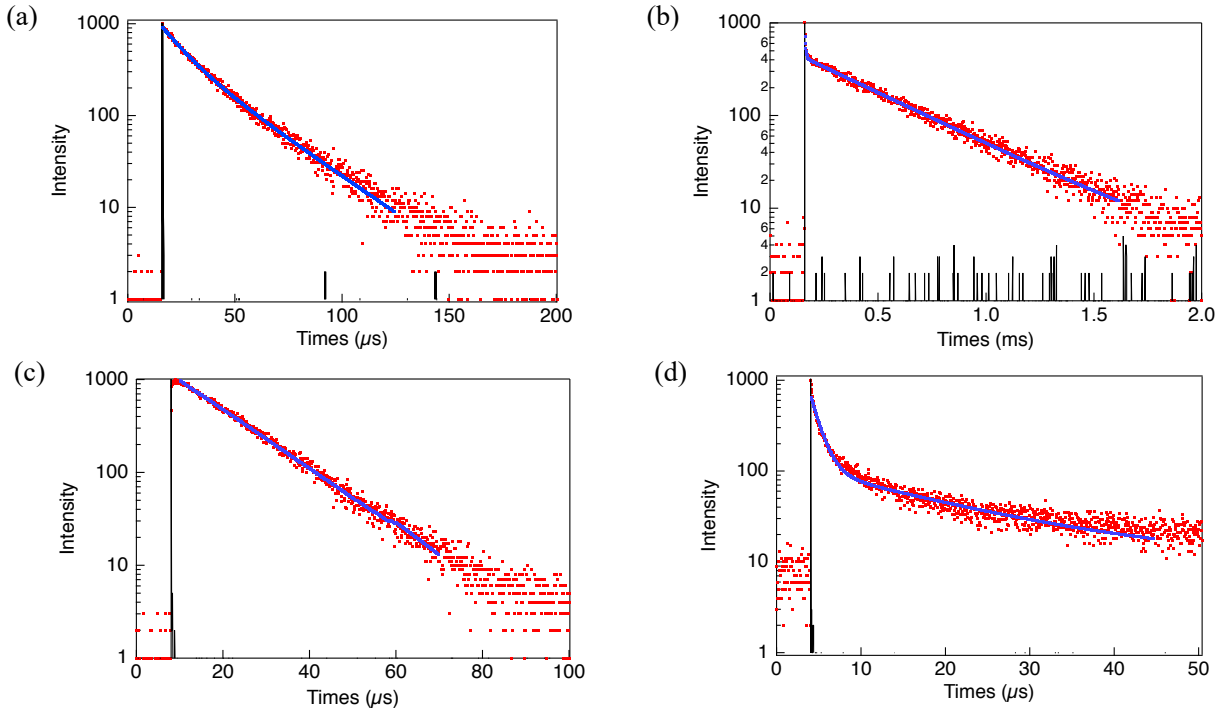

Fig. S12 Luminescence decay profiles of **CP** crystals: (a) **CP-B** at 423 nm**,** (b) **CP-G** at 500 nm, (c) **CP-Y** at 560 nm, and (d) **CP$_{ground}$** at 500 nm (red, observed decay; blue, fitting curve; black, instrument response function; λ_{ex} = 340 nm).

Table S4. Luminescence lifetime of **CP** in crystals. [a]

	λ_{obs} (nm)	τ (μs)
CP-B	423	11 (50%); 27 (50%)
CP-G	500	4 (52%); 389 (48%)
CP-Y	560	13
CP$_{ground}$	500	1 (86%); 16 (14%)

[a] Abbreviations: λ_{obs}, observation wavelength for luminescence decay. τ, luminescent lifetime. λ_{ex} = 340 nm for all measurements.

Luminescence of crystal polymorphs at low temperature

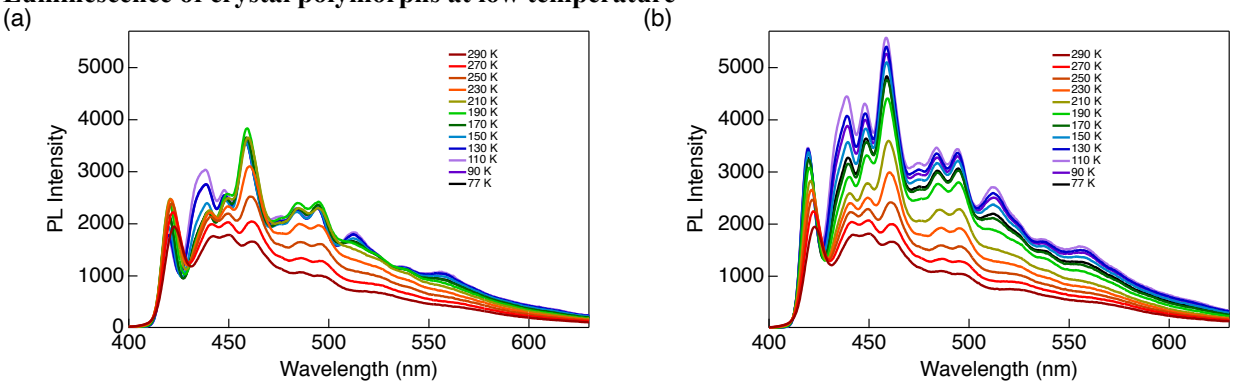

Fig. S13 Temperature-dependent luminescence of **CP-B** crystals under excitation at (a) 320 nm and (b) 373 nm.

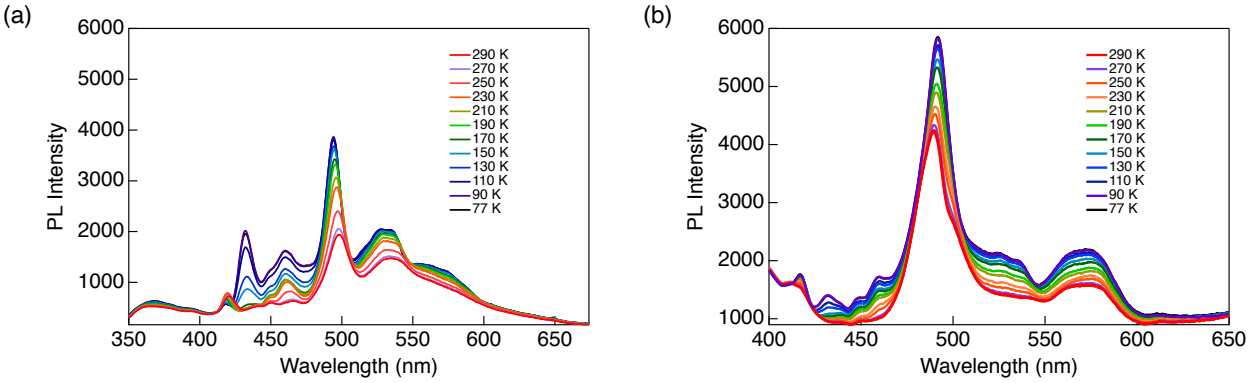

Fig. S14 Temperature-dependent luminescence of **CP-G** crystals under excitation at (a) 320 nm and (b) 373 nm.

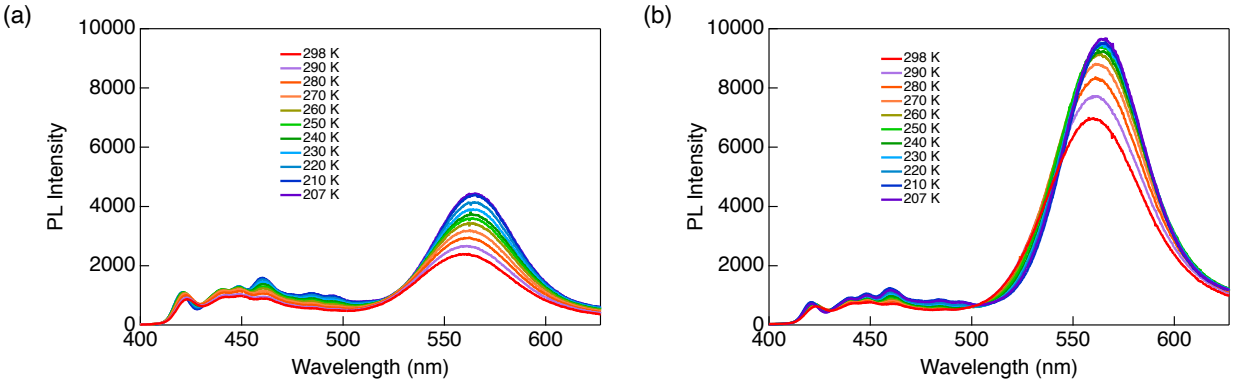

Fig. S15 Temperature-dependent luminescence of **CP-Y** crystal under excitation at (a) 320 nm and (b) 373 nm.

5. PXRD analysis

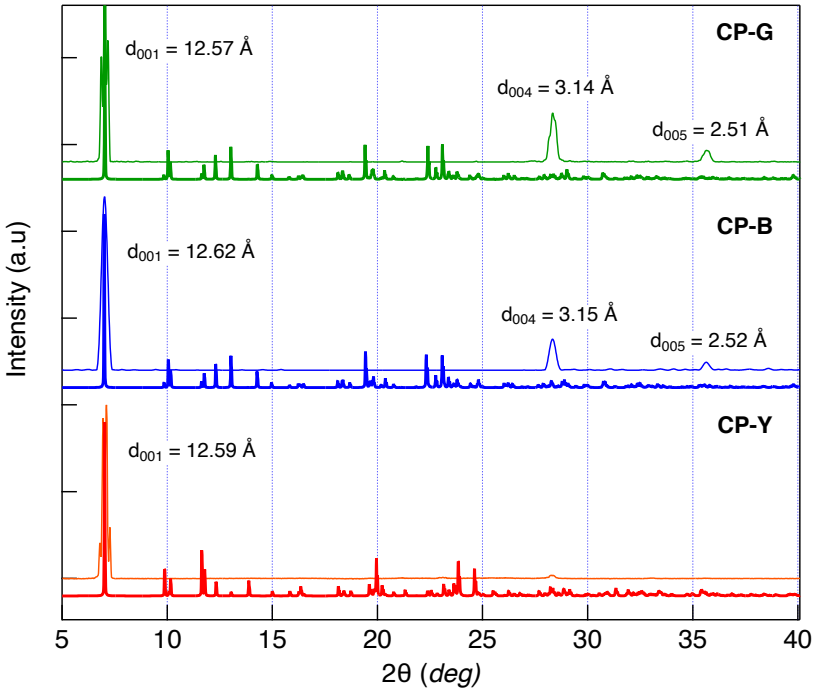

Fig. S16 PXRD patterns of bulk crystals of **CP-G** and **CP-B** (thin lines) with corresponding simulated single crystal XRD pattern (bold lines). The PXRD peaks of bulk crystals were indexed using the single crystal data. The observed PXRD pattern of bulk crystals shows preferential molecular orientation, resulting in only three reflections (d001, d004, and d005) being observable while other peaks become negligible.[1] This orientation amplifies the (00l) reflections while removing the others. Additionally, the PXRD pattern of **CP-Y** bulk crystal is included for comparison.

6. TD-DFT Calculation

The molecular orbitals, transition energies, and oscillator strengths (*f*) of the complexes were calculated using time-dependent density functional theory (TD-DFT). The TD-DFT calculations for the dimers suggested that electronic transitions from the ground state (S_0) to the singlet excited state (S_n) falling within the UV range, spanning between 266 and 319 nm, attribute to both LMCT and LMMCT transitions (Table S5, Fig. 6b, and Figs. S17–S18). The excitation energies of the triplet excited states were calculated from the same dimers, indicating that the S_0–T_1 transitions are located at 409 nm, 372 nm, and 412 nm for **CP-B**, **CP-G**, and **CP-Y**, respectively (Table S6). In case of the monomer, the S_0–S_n transitions are located at 274 and 347 nm (Table S7), and this calculated result roughly aligns with the absorption spectra of the complex in dilute solution (Fig. 2). Furthermore, the calculations suggested that an intramolecular LMCT transition occurred in the monomer (Fig. S19).

Table S5. Transition, oscillator strengths (*f*), and excitation wavelength (λ) for S_0–S_n excitation calculated for **CP-B**, **CP-G**, and **CP-Y** dimer.

	Transition	*f*	λ (nm)
CP-B	HOMO−1 → LUMO	0.5492	318.88
	HOMO → LUMO+2	0.5001	281.78
CP-G	HOMO−1 → LUMO	0.9069	266.47
	HOMO → LUMO+2	0.3031	250.27
CP-Y	HOMO−1 → LUMO	0.5163	303.93
	HOMO → LUMO+2	0.4996	267.54

Table S6. Excitation wavelength (λ) for the lowest S_0–T_n transition calculated for **CP-B**, **CP-G**, and **CP-Y** dimer.

	λ (nm)
CP-B	408.93
CP-G	372.01
CP-Y	412.03

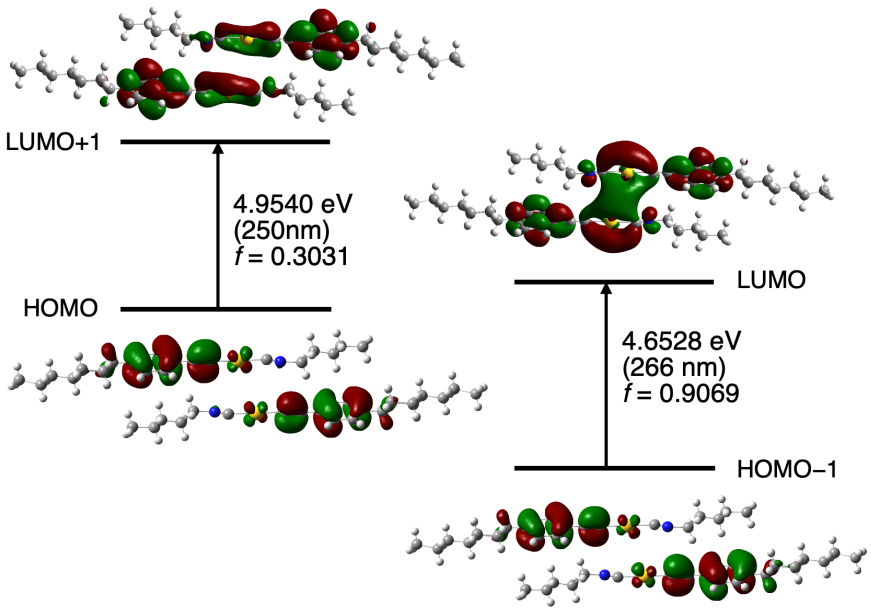

Fig. S17 Molecular orbitals of **CP-G** dimer computed using DFT with B3LYP and 6−311+G(d,p), except Au atoms, for which SDD set was employed.

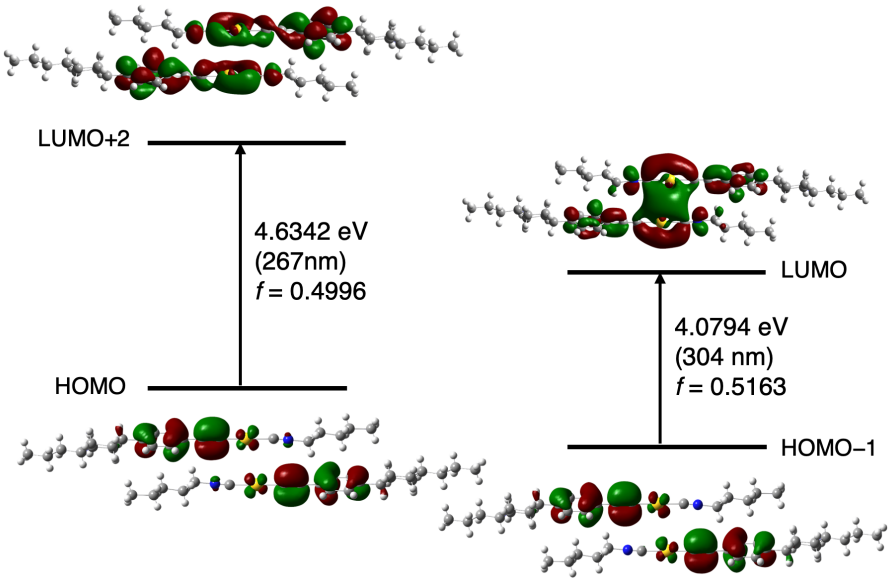

Fig. S18 Molecular orbitals of **CP-Y** dimer computed using DFT with B3LYP and 6−311+G(d,p), except Au atoms, for which SDD set was employed.

Table S7. Transition, oscillator strengths (f), and excitation wavelength (λ) for S_0–S_n excitation calculated for **CP** monomer.

	Transition	f	λ (nm)
CP	HOMO → LUMO	0.3843	347.36
	HOMO → LUMO+2	0.4278	273.93

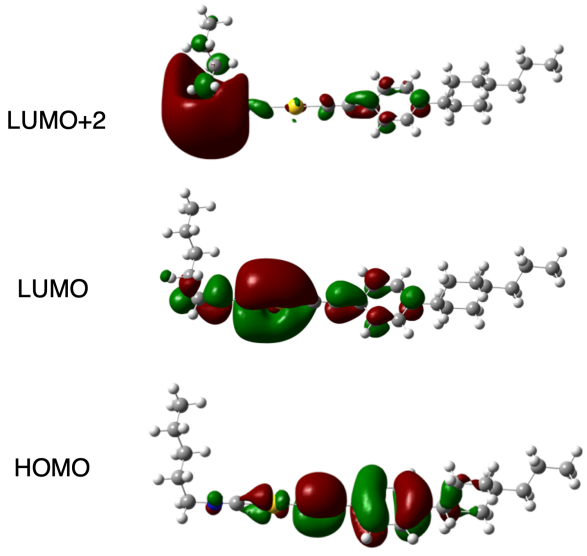

Fig. S19 Molecular orbitals of **CP** monomer computed using DFT with B3LYP and 6−311+G(d,p), except Au atoms, for which SDD set was employed.

7. Mechanochromic luminescence

Luminescence of ground sample

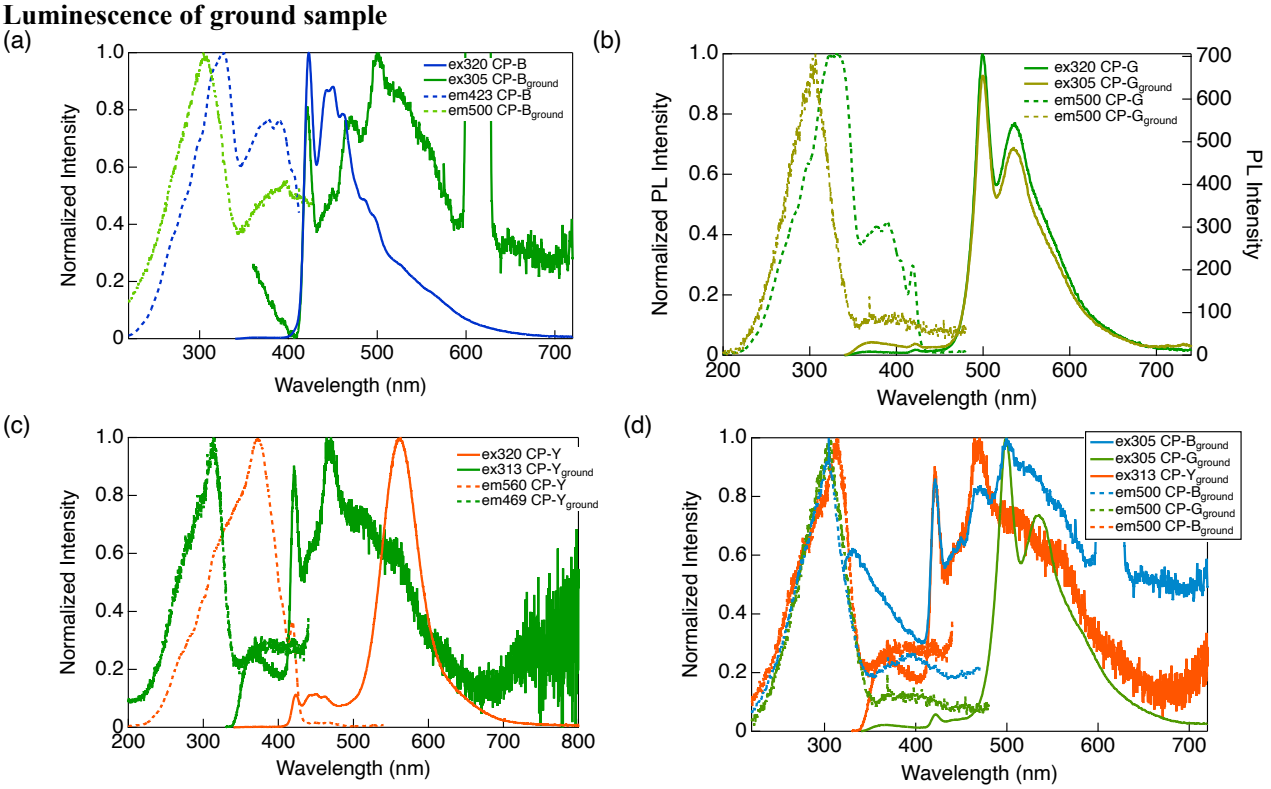

Fig. S20 Emission and excitation spectra of (a) **CP-B**, (b) **CP-G**, and (c) **CP-Y** of bulk and ground crystals. (d) Overlay of ground crystal polymorphs for comparison.

SEM images of ground CP crystals

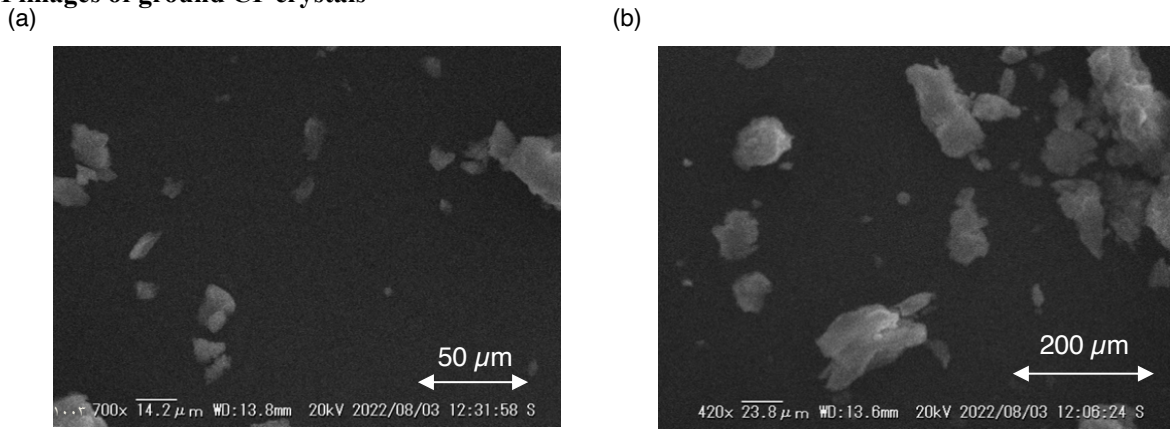

Fig. S21 SEM images of **CP-B** and **CP-G** in ground crystals.

8. Luminescence in LC phase

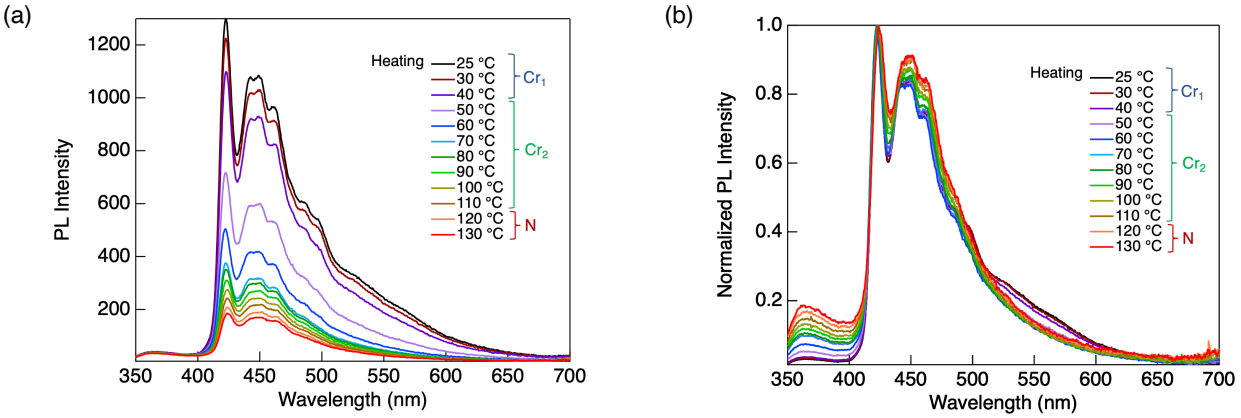

Fig. S22 (a) Photoluminescence spectra of **CP-B** at various temperature during heating process and (b) the normalized spectra. λ_{ex} = 320 nm.

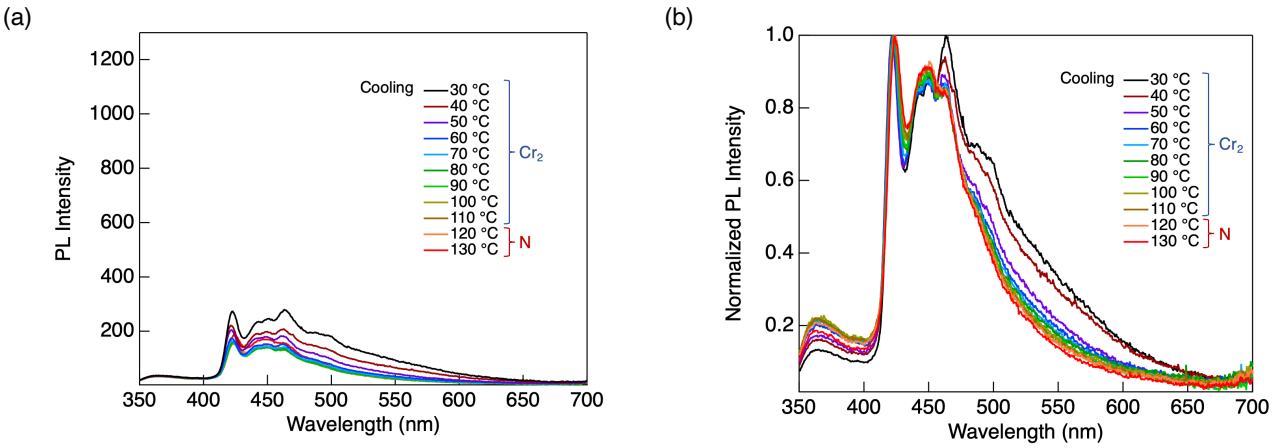

Fig. S23 (a) Photoluminescence spectra of **CP-B** at various temperature during cooling process and (b) the normalized spectra. λ_{ex} = 320 nm.

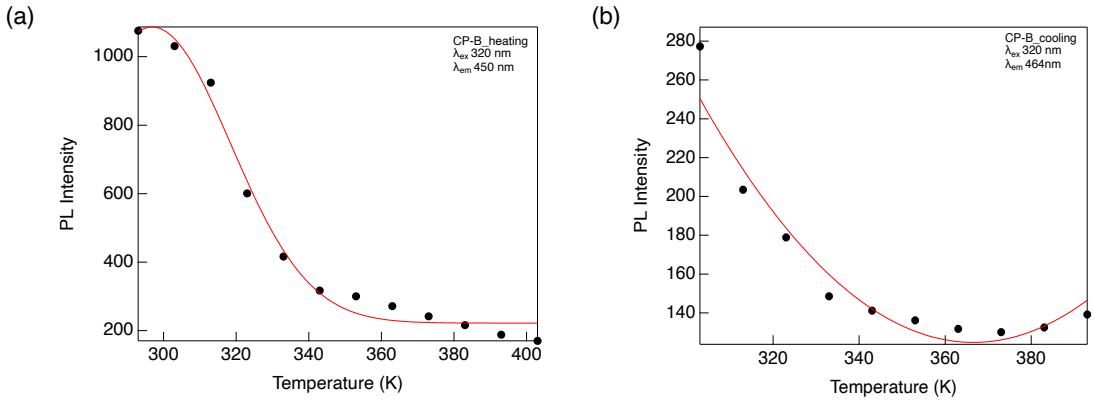

Fig. S24 Temperature-dependent luminescence intensity for **CP-B** during (a) heating and (b) cooling processes. λ_{ex} = 320 nm, λ_{em} = 450 nm for heating and λ_{em} = 464 nm for cooling.

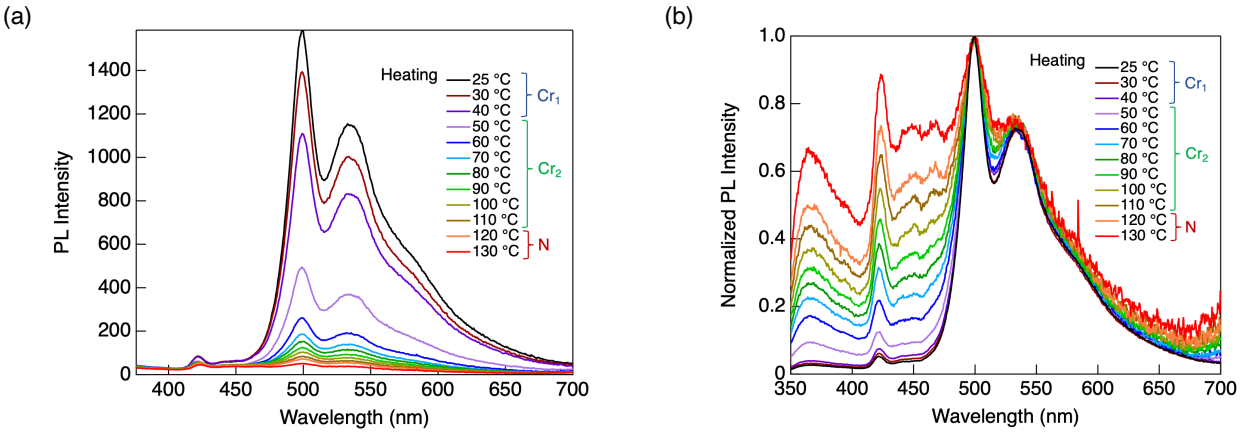

Fig. S25 (a) Photoluminescence spectra of **CP-G** at various temperature during heating process and (b) the normalized spectra. (λ_{ex} = 320 nm).

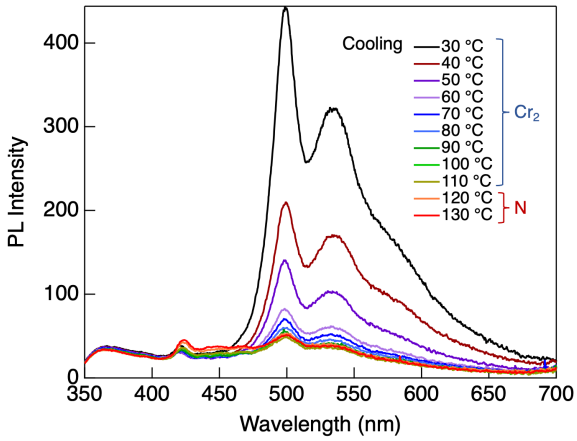

Fig. S26 Photoluminescence spectra of **CP-G** at various temperature during cooling process (λ_{ex} = 320 nm).

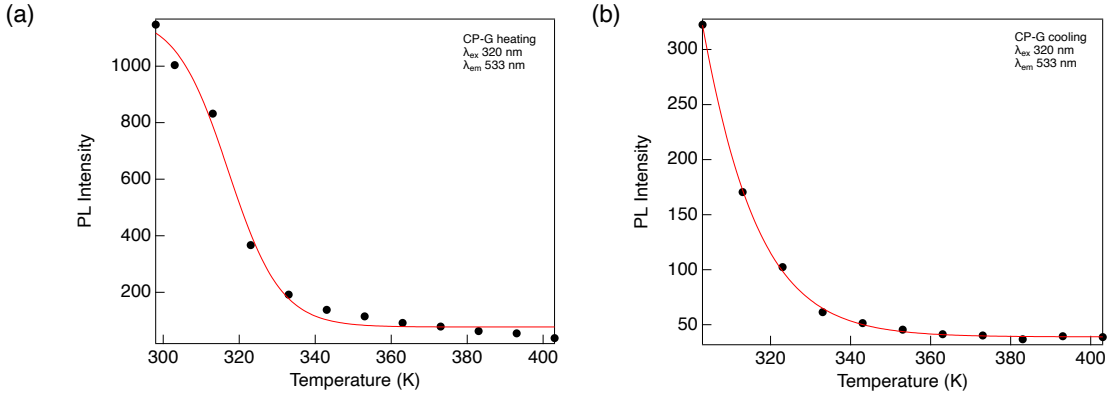

Fig. S27 Temperature-dependent luminescence intensity for **CP-G** during (a) heating and (b) cooling processes. λ_{ex} = 320 nm, λ_{em} = 533 nm.

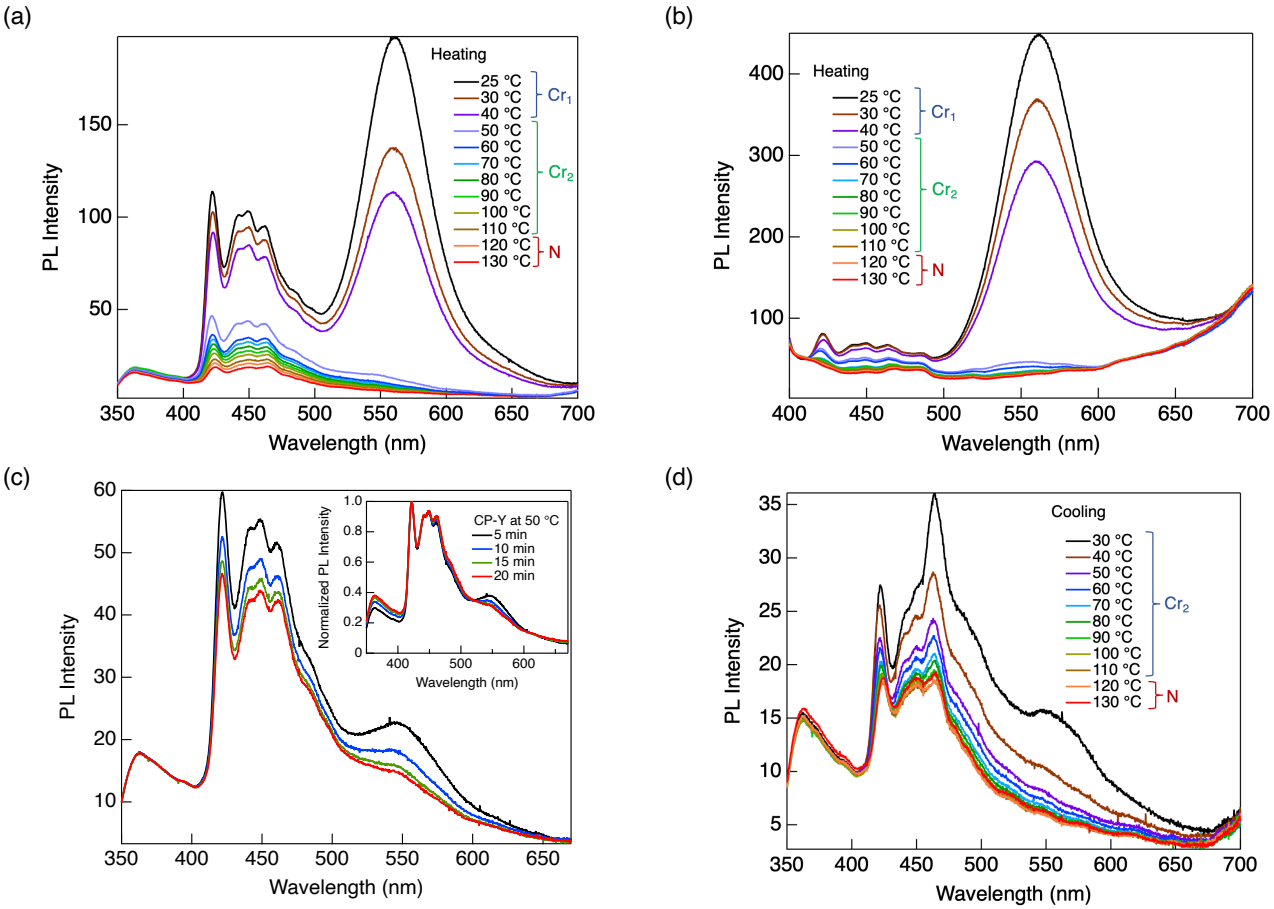

Fig. S28 Photoluminescence spectra and the normalized spectra of **CP-Y** at various temperature during (a, b) heating, and (d) cooling processes under excitation at 320 nm for (a, d) and 370 nm for (b). (c) Photoluminescence spectra of **CP-Y** during heating process at 50 °C varying holding times under excitation at 320 nm, showing a decrease in relative emission intensity at 560 nm with prolonged holding time due to ongoing phase transition.

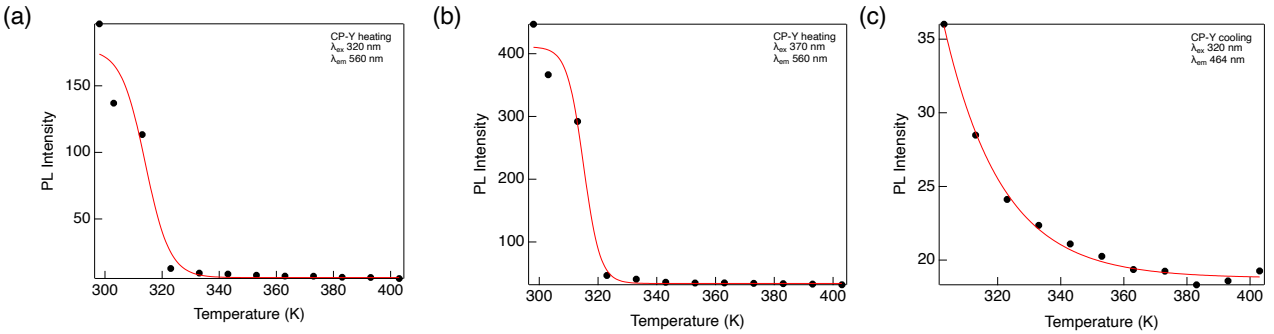

Fig. S29 Temperature-dependent luminescence intensity for **CP-Y** during (a, b) heating and (c) cooling processes under excitation at 320 nm for (a, c) and 370 nm for (b). λ_{em} are 560 nm for heating and 464 nm for cooling.

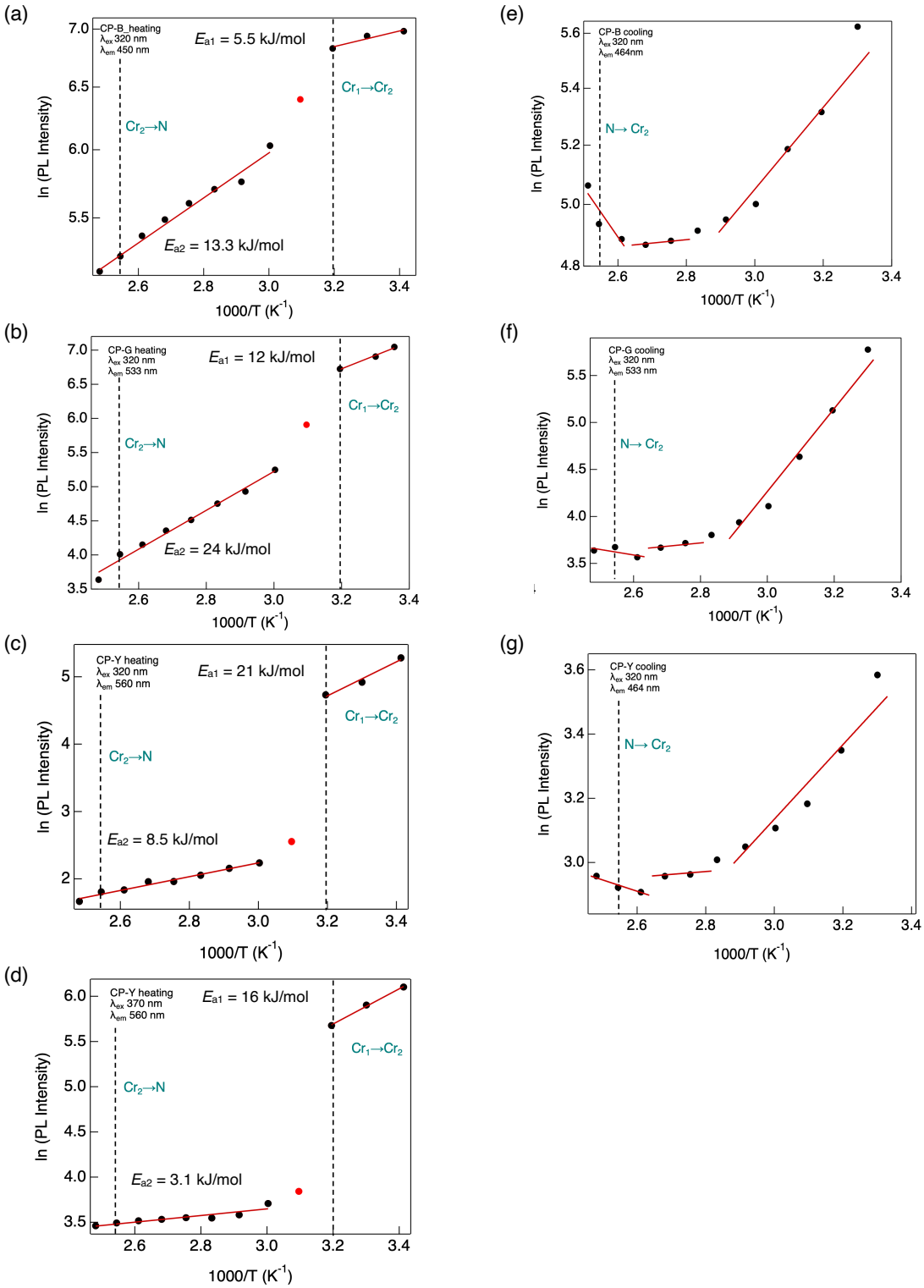

Fig. S30 Arrhenius fit of luminescence intensity versus temperature for **CP** polymorphs during (a–d) heating and (e–g) cooling processes. λ_{ex} = 320 nm for all measurements, except for (d), where 370 nm excitation was utilized. During heating, λ_{em} were set at 450 nm, 533nm, and 560 nm for **CP-B**, **CP-G**, and **CP-Y**, respectively. For cooling, λ_{em} was 533 nm for **CP-G** and 464 nm for other **CP** polymorphs. Dashed line indicates the phase transition temperature. Red dot indicates omitted data from fitting due to high error value (see Fig. 28c, and explanation in the main text).

References

[1] J. Binns, C. Darmanin, C. M. Kewish, S. K. Pathirannahalge, P. Berntsen, P. L. R. Adams, S. Paporakis, D. Wells, F. G. Roque, B. Abbey, G. Bryant, C. E. Conn, S. T. Mudie, A. M. Hawley, T. M. Ryan, T. L. Greaves and A. V. Martin, *IUCrJ*, 2022, **9**, 231.